



Geophysical Research Letters

RESEARCH LETTER

10.1029/2019GL085291

Key Points:

- A physics-constrained machine learning model of evapotranspiration (hybrid model) is developed and trained using the FLUXNET 2015 data set
- The evapotranspiration retrieved by the hybrid model is as accurate as pure machine learning model and also conserves surface energy balance
- The hybrid model better reproduces extremes and thus better extrapolates compared to the pure machine learning approach

Supporting Information:

- Supporting Information S1
- Figure S1
- Table S1

Correspondence to:

P. Gentine and G. Y. Qiu,
pg2328@columbia.edu;
qiyug@pkusz.edu.cn

Citation:

Zhao, W. L., Gentine, P., Reichstein, M., Zhang, Y., Zhou, S., Wen, Y., et al. (2019). Physics-constrained machine learning of evapotranspiration. *Geophysical Research Letters*, 46, 14,496–14,507. <https://doi.org/10.1029/2019GL085291>

Received 6 SEP 2019

Accepted 5 DEC 2019

Accepted article online 9 DEC 2019

Published online 23 DEC 2019

Physics-Constrained Machine Learning of Evapotranspiration

Wen Li Zhao^{1,2}, Pierre Gentine², Markus Reichstein^{3,4}, Yao Zhang², Sha Zhou², Yeqiang Wen^{2,5}, Changjie Lin⁵, Xi Li⁶, and Guo Yu Qiu¹

¹School of Environment and Energy, Peking University Shenzhen Graduate School, Peking University, Shenzhen, China,

²Department of Earth and Environmental Engineering, Columbia University, New York, NY, USA, ³Department of Biogeochemical Integration, Max Planck Institute for Biogeochemistry, Jena, Germany, ⁴Michael-Stifel-Center Jena for Data-Driven and Simulation Science, Jena, Germany, ⁵State Key Laboratory of Hydroscience and Engineering, Department of Hydraulic Engineering, Tsinghua University, Beijing, China, ⁶Institute of Water Sciences, College of Engineering, Peking University, Beijing, China

Abstract Estimating ecosystem evapotranspiration (ET) is important to understanding the global water cycle and to study land-atmosphere interactions. We developed a physics constrained machine learning (ML) model (hybrid model) to estimate latent heat flux (LE), which conserves the surface energy budget. By comparing model predictions with observations at 82 eddy covariance tower sites, our hybrid model shows similar performance to the pure ML model in terms of mean metrics (e.g., mean absolute percent errors) but, importantly, the hybrid model conserves the surface energy balance, while the pure ML model does not. A second key result is that the hybrid model extrapolates much better than the pure ML model, emphasizing the benefits of combining physics with ML for increased generalizations. The hybrid model allows inferring the structural dependence of ET and surface resistance (r_s), and we find that vegetation height and soil moisture are the main regulators of ET and r_s .

Plain Language Summary A physics constrained machine learning model is developed using the FLUXNET2015 Tier 1 data set. This new approach is able to effectively retrieve latent heat flux while constraining energy conservation in the surface energy budget. This hybrid model has better performance in extrapolation than a pure machine learning model.

1. Introduction

Evapotranspiration (ET) is a key component of the global hydrological cycle and of the interaction between the surface water and energy cycles (Katul et al., 2012; Wang & Dickinson, 2012; Xu et al., 2019; Zou et al., 2019). Accurate ET estimation is critical to solving global hydrological problems (Morillas et al., 2013; Zhang et al., 2016; Zhang et al., 2019). Two main types of models have been developed for ET estimation. The first, physics-based models take advantage of an explicit physical representation and can conserve energy, but need to empirically estimate some parameters like surface resistance, which is a challenge especially at the global scale. This type of models can generally be classified into three categories: Penman-Monteith (PM) or Priestley-Taylor models (Cleugh et al., 2007; Leuning et al., 2008; Mu et al., 2007; Mu et al., 2011; Peng et al., 2019; Yao et al., 2015; Zhang et al., 2010), surface energy balance models (Bastiaanssen et al., 1998; Li, Kustas, et al., 2019; McCabe & Wood, 2006; Norman et al., 1995; Qiu, 1996; Qiu et al., 1996; Wang et al., 2016), and empirical vegetation index-land surface temperature triangle/trapezoidal models (Carlson & Petropoulos, 2019; Jiang & Islam, 1999; Long & Singh, 2012; Yang & Shang, 2013; Zhu et al., 2017). The second group of models include statistical models, which can be empirical or semi-empirical model (Jung et al., 2009; Jung et al., 2010; Tramontana et al., 2016; Wang et al., 2007) or based on machine learning (ML) techniques (Alemohammad et al., 2017; Feng et al., 2017; Gocic et al., 2016; Granata, 2019; Jung et al., 2009; Tang et al., 2018). These statistical models can be more easily applied, especially at the global scale, but can behave poorly outside of their calibration range and predict climate anomalies, such as extremes (Tramontana et al., 2016). Another major issue is that those models typically do not conserve the surface energy budget, which can be a major issue for model assessment of the various surface flux components of the surface energy balance (net radiation, sensible and latent heat fluxes [LEs], and ground heat flux) or for implementation with a coupled atmospheric model.

In recent years, with the large accumulation of satellite data and ground observation data, ML algorithms have been used more widely for ET estimation (Alemohammad et al., 2017; Chaney et al., 2016; Jung et al., 2009; Ke et al., 2016; Torres et al., 2011; Tramontana et al., 2016; Yang et al., 2006). Yet, physics-based models can make use of scientific theory and tend to have better generalization and interpretability (Reichstein et al., 2019), yet still have limitations as they do not optimally extract information from the data. In contrast, ML models can make full use of the available data and have consistency with the input data sets, yet generally lack physical constraints (e.g., energy conservation, and diffusion laws) and interpretability (Reichstein et al., 2019). Recent studies suggest that physics-based models and ML models will not replace each other, but instead that a most promising and also challenging approach could come from combining ML and physical modeling (Reichstein et al., 2019). However, it is still unclear whether hybrid models, that is, the integration of physics-based model and ML model, can have the advantages of both physical and statistical models for predicting ET.

To answer this question, we here develop the first physics-constrained ML model of ET, which combines an energy-conserving PM-like equation (Gao, 1988; Monteith, 1965; Penman, 1948) and a ML model. Surface resistance (r_s), regarded as a submodel in the physical PM equation, is difficult to quantify and is the main unknown term of PM. Most researchers use empirical or semi-empirical methods to estimate r_s ; however, little theoretical basis (for example, on the biological regulation process of stomata) is employed so that the modeled ET varies widely across models according to the structural form of the chosen r_s . A hybrid model can be built by targeting r_s with ML instead of the full ET while ensuring energy conservation and meeting the physical constraint that ET is downgradient of vapor pressure, that is, a turbulent diffusion process. Such a hybrid model could in turn optimally learn from the data while respecting physical laws. This hybrid model can then benefit from both the strengths of physical modeling (theoretical foundations and interpretability) and ML (data adaptiveness) (Reichstein et al., 2014; Reichstein et al., 2019). The hybrid model proposed in this paper is aimed at predicting ET accurately and more importantly to conserve the surface energy budget and to respect the fact that ET is a (turbulent) diffusive process. This model can in turn be used to infer if and in which way relevant variables (e.g., soil moisture [SM], air temperature, vegetation height, and relative humidity [RH]) control r_s and ET. Further, we test whether the hybrid model can better reproduce extremes and thus can better generalize outside of the range of the training data set compared to the regular ML algorithm.

2. Data

In this study, we used 82 eddy covariance sites from the FLUXNET 2015 tier 1 data set (<https://fluxnet.fluxdata.org/data/download-data/>). The underlying surfaces cover nine PFTs (plant function type) based on the International Geosphere-Biosphere Programme vegetation classification scheme (Loveland et al., 1999), including evergreen needleleaf forests (ENF), evergreen broadleaf forests, deciduous broadleaf forests, croplands (CRO), grasslands (GRA), savannas, woody savannas, closed shrublands, and mixed forests (MF).

The sampling frequency is half hourly. The data filter procedure follows previous typical ones (e.g., Li, Gentile, et al., 2019; Lin et al., 2018; Zhou et al., 2015, 2016), which can be summarized as follows: First, only measured and good-quality gap-filled data (Reichstein et al., 2005) were selected. Second, we removed the data that were sampled during rainy days and the following day to avoid issues with rain interception and sensor saturation at high RH (Medlyn et al., 2011). Third, only daytime data were used for model calculation; therefore, the data periods with sensible heat larger than 5 W/m^2 and incoming shortwave radiation larger than 50 W/m^2 were selected to avoid stable boundary layer conditions. Fourth, negative gross primary production, LE, and vapor pressure deficit (VPD) were excluded. Finally, only the half-hourly data with carbon dioxide concentration (Ca), net radiation (R_n), and ground heat flux (G) between 5th and 95th percentiles for Ca, R_n , and G , respectively, were used. All the half-hourly LE data from the FLUXNET 2015 Tier 1 data set were imposed and corrected to achieve energy balance closure using a Bowen ratio method (Barr et al., 2006; Liu et al., 2011; Twine et al., 2000; Xu et al., 2013) when the energy balance closure, that is, $(\text{LE} + \text{H})/(R_n - G)$, was less than 0.8.

In our study, we used measured surface SM value (if no upper surface SM was available, the lower surface one was used) from the FLUXNET 2015 Tier 1 data set. Upper surface SM is usually strongly temporally

correlated with deeper layers, which mitigates the issue of not having deep observations (Albergel et al., 2008; Ford et al., 2014; Qiu et al., 2014).

The fraction of photosynthetically active radiation (fpar) information was taken from simultaneous Moderate Resolution Imaging Spectroradiometer products MCD15A3H using the Global Subset Tool (<https://modis.ornl.gov/cgi-bin/MODIS/global/subset.pl>). The temporal resolution is 4 days. Fpar does not change significantly within 4 days, so we used this fpar value for the half-hourly input of the algorithms.

Vegetation height for every flux site was estimated using the method of (Pennypacker & Baldocchi, 2016) (see Table S1).

3. Methodology

3.1. Artificial Neural Network

A feedforward Artificial Neural Network (ANN) was used to estimate LE (Alemohammad et al., 2017) based on 13 variables including fpar, SM, VPD, PFT, air temperature (Ta), carbon dioxide concentration (Ca), WS, atmospheric surface pressure, RH, net radiation (R_n), soil heat flux (G), PAR (incoming photosynthetic photon flux density from FLUXNET 2015 data set is used here instead), and vegetation height (h_canopy) (detailed information of these variables is summarized in supporting information Table S1). All input variables except PFT were normalized by the mean and standard deviation to zero mean and one unit to accelerate the learning pace. For PFT, we kept the original category value (1, 2, 3, 4, 5, 6, 7, 8, 9) as input. The optimal structure of the ANN used here is a network consisting of six layers (see below): (1) an input layer that directly connects to the input data, (2) five hidden layers and 64 neurons for each layer, and (3) an output layer with one neuron that produces target estimates. The activation function is a rectified linear unit, relu.

We first shuffle the entire data set randomly across time and sites and then separate the whole data set into three subsets, as typically done: a training, a validation, and a test data set with ratios of 64%, 16%, and 20%. We repeat the training for several ANNs with an increasing number of hidden layers from 1 to 15 and an increasing number of neurons, for example, 8, 16, 32, 64, 128, to avoid overfitting (Figure S5). As a result, the ANN with 5 hidden layers and 64 neurons in each hidden layer is the best performing model in terms of mean square errors while minimizing the number of degrees of freedom based on an Akaike Information Criterion (AIC) (see details in section 3.4). Early stopping is used to avoid overfitting.

3.2. Pure ML Model

In the pure ML case, the ANN is used to predict LE directly (Figure 1a). The mean squared error (MSE) of LE is used as the loss function in the training process. We emphasize that this pure ML cannot exactly conserve the surface energy budget (if the ANN is also used to estimate sensible heat flux H , given R_n and G , as seen in Figure 2e1)—with a large root-mean-square error (RMSE) of 62.42 W/m^2 in the surface energy budget larger than typical ground heat flux values.

3.3. Hybrid Model

We then build a hybrid model integrating an ANN and a modified PM equation to predict LE (Figure 1b). The ANN is set to predict the logarithm value of r_s instead of r_s because it is more normally distributed. The typical PM equation is based on a big leaf model that uses the linearization of the Clausius-Clapeyron relationship, along with the surface energy budget, and therefore does not exactly conserve energy because of the curvature of Clausius-Clapeyron. To mitigate this issue, we use a second-order Taylor approximation of Clausius-Clapeyron and develop a corrected second-order Penman-Monteith equation (Gao, 1988; Monteith, 1965; Penman, 1948; see details in Text S1). This equation is then used in the loss function to make sure that the LE predictions by the hybrid model constrain the surface energy balance and the diffusion-like process of ET (see details in Text S1).

3.4. Model Selection

Using a subset of 13 variables (supporting information in Table S1) as input for the ANNs produces 8,191 input variable combinations. We test different variable combinations as inputs (Text S2) for the pure ML model and hybrid model. Then we use the AIC (Akaike, 1974; Akaike et al., 1998; Anders & Korn, 1999; Arifovic & Gençay, 2001) to select the best hybrid model across PFTs:

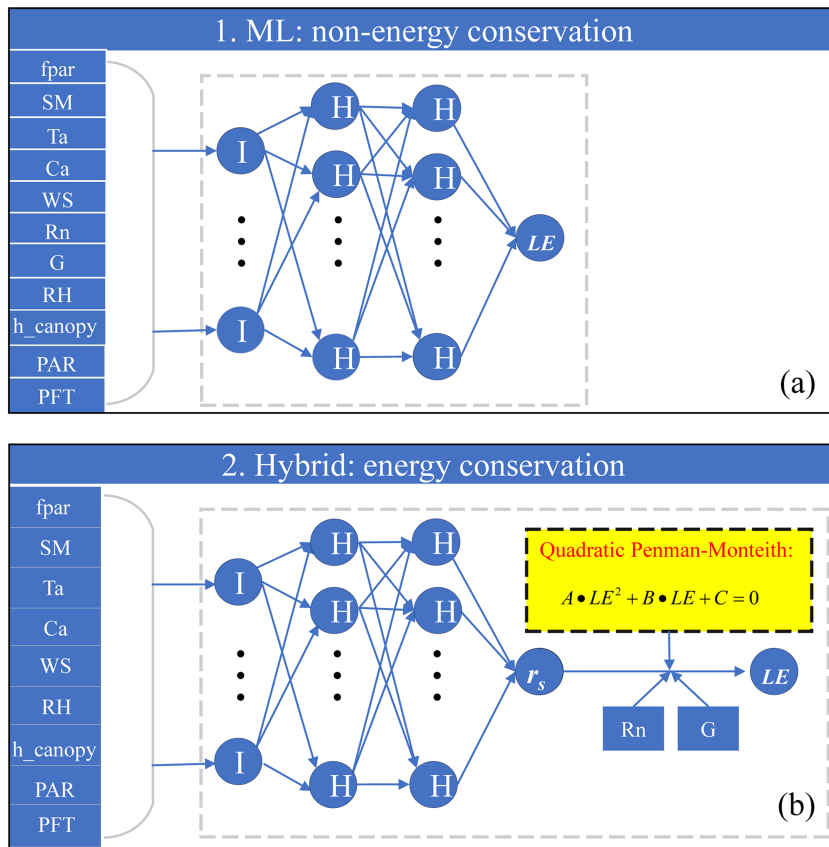


Figure 1. Flow chart of the (a) nonenergy-conserving, pure machine learning model, and (b) energy-conserving, hybrid model. The letter I represents Input layer, H represents hidden layers, LE is latent heat flux, r_s is surface resistance, fpar is the fraction of photosynthetically active radiation, SM is soil moisture, Ta is air temperature, Ca is Carbon dioxide concentration, WS is wind speed, RH is relative humidity, h_canopy is vegetation height, PAR is incoming photosynthetically active radiation (incoming photosynthetic photon flux density from FLUXNET 2015 dataset is used here instead), PFT is plant function type, R_n is net radiation, and G is soil heat flux (also shown in supporting information Table S1). A, B, C are the coefficients of the quadratic Penman-Monteith equation, which have been described clearly in the following section 3.3. The aerodynamic resistance's calculation procedures are described in section 3.3.

$$AIC = \ln(MSE) + \frac{2q}{n} \quad (1)$$

where MSE is mean squared error, q is the estimable parameters in neural network, and n is the number of observations in the training data set.

4. Results and Discussion

4.1. Comparisons Between LE Predictions of Hybrid Model and Pure ML Model

The best hybrid model selected using the AIC is the one with input variables: fpar, SM, Ta, Ca, WS, RH, h_canopy, PAR, and PFT. Due to the additional necessity of using R_n and G in the PM equation, we also use R_n and G as additional inputs in the pure ML algorithm for a fair comparison.

The LE predictions by the hybrid model (LE_hybrid) has a slightly lower mean absolute percent error (MAPE) of 20.92% compared to 20.96% for the pure ML model (LE_ML) on the test data set (Figures 2b1 and 2c1), but both models have very similar skills. The nonbiased linear regression shows that LE_hybrid slightly underestimates the observations with a slope of 1.06, R^2 of 0.78, MAE and RMSE of 37.12 and 51.86 W/m², while LE_ML has a slope of 1.00 with R^2 of 0.81, MAE and RMSE of 34.31 and 46.73 W/m² on the validation data set. Even though the pure ML algorithm LE_ML slightly better fits the data, it does

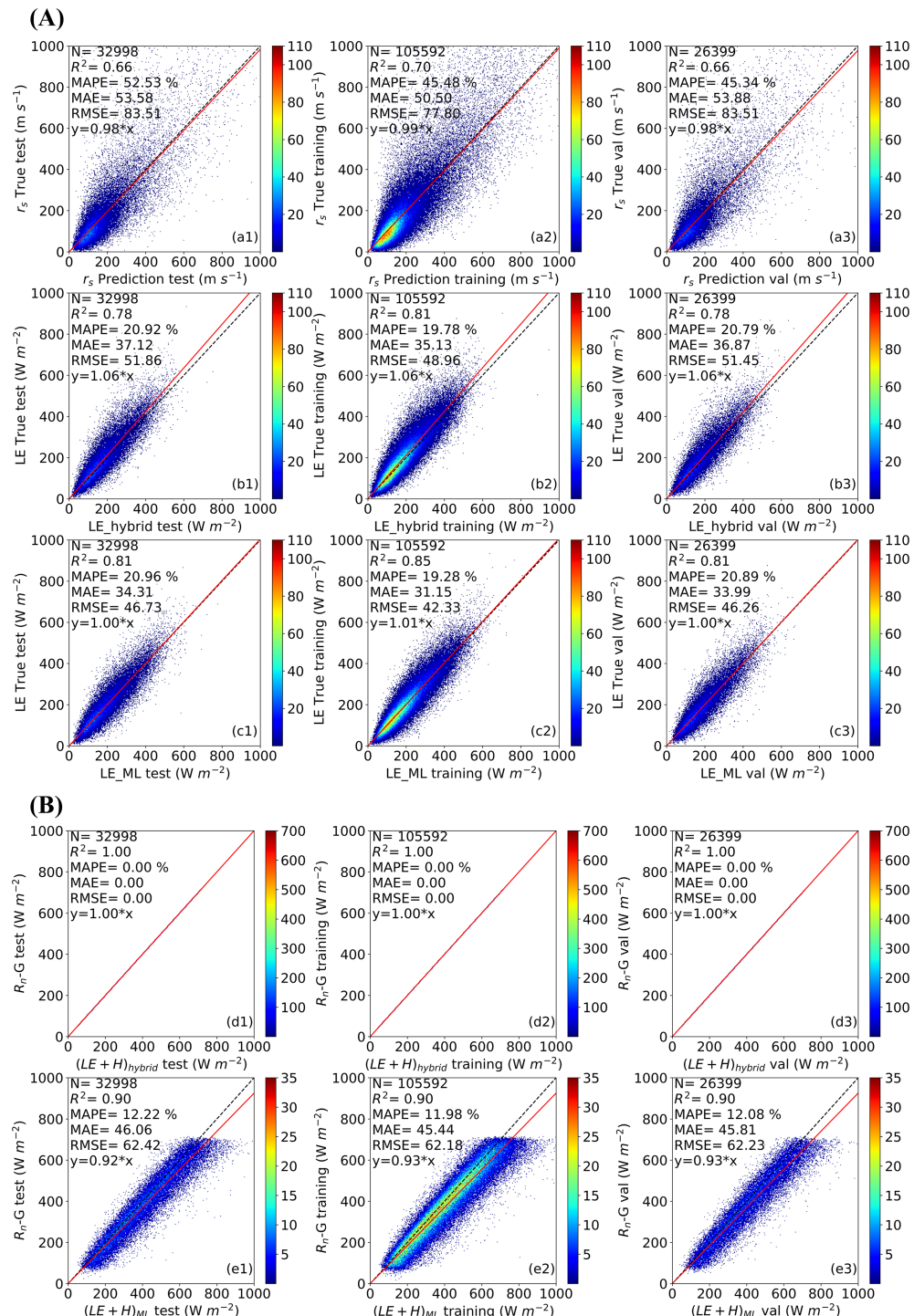


Figure 2. Performance of the hybrid and pure machine learning models in predicting latent heat flux (LE) and energy conservation. (a) The half-hourly hybrid model retrieval of surface resistance (r_s) and LE and pure machine learning model retrieval of LE over the test, training, and validation data set. The letters a, b, and c represent the r_s predictions by the hybrid model, corresponding LE predictions by the hybrid model, and LE predictions by the pure machine learning model, respectively. The numbers 1, 2, and 3 indicate whether the test, training, and validation data set is used, respectively. (b) Performance of the surface energy conservation for the half-hourly hybrid model and pure machine learning model retrieval of LE plus H over the test, training, and validation data sets. Panels d and e represent $(LE + H)$ the predictions by the hybrid and pure machine learning models, respectively. The number 1, 2, and 3 indicate the test, training, and validation data set, respectively. The density of scatter points is represented using shading colors. The diagonal black dashed line depicts the 1:1 line, and the red solid line depicts the nonbiased linear regression line. N, R^2 , MAPE, MAE, and RMSE represent the number of points, coefficient of determination, mean absolute percent error, mean absolute error, and root-mean-square error, respectively. We note that data points are perfectly on the 1:1 line for the hybrid model in d1, d2, and d3; the nonbiased regression line is $y = x$ indicating near-perfect surface energy budget closure.

not conserve the surface energy budget and can lead to large surface energy imbalances with an RMSE of 62 W/m² (Figure 2e).

In order to verify the robustness of the results, we repeated 50 times the NN fits of the hybrid and pure ML models. The results show that in most cases, the hybrid model has a lower MAPE than the pure ML model (40 times) (Figure S1a). Yet, the pure ML ET always yields a higher R^2 than the hybrid model (Figure S1b). This should come as no surprise as the pure ML model is targeted at only minimizing the MSE of LE, without the additional constraint of satisfying the energy budget, which should by definition increase the MSE. For the training and validation data sets, the hybrid model has a slightly lower than yet similar performance to the pure ML model with R^2 , slope, MAPE, MAE, and RMSE of 0.81, 1.06, 19.78%, 35.13 W/m², and 48.96 W/m compared to 0.85, 1.01, 19.28%, 31.15 W/m², and 42.33 W/m² for the training data set (Figures 2b2 and 2c2), and 0.78, 1.06, 20.79%, 36.87 W/m², and 51.45 W/m² compared to 0.81, 1.00, 20.89%, 33.99 W/m², and 46.26 W/m² for the validation data set (Figures 2b3 and 2c3). Cross validations were also used to ensure that our results were stable (Text S3).

4.2. Interpretation of Surface Resistance Predictions by the Hybrid Model

The hybrid model can predict r_s accurately and therefore can be used to systematically understand the functional dependence of r_s on SM, Ta, Ca, RH, PAR, and VPD (Figure 3), at the ecosystem scale, which has been a long-term challenge. As expected, r_s decreases sharply as SM and RH increase (Figures 3a and 3d), while it increases with Ta and VPD (Figures 3b and 3f). For PAR and Ca, the relationship between r_s and these two variables shows large variations (Figures 3c and 3e), because other environmental factors can be covarying at the same time—for instance, temperature can increase during reduced cloud cover while PAR is also increasing, leading to the large observed variations for given PAR values (Figure 3e). Yet, overall, r_s decreases with PAR and is not as parabolic as previously thought (Jarvis, 1976). Increased ambient CO₂, Ca, in turn increases r_s across PFTs, emphasizing the role of CO₂ effects on stomatal conductance at the ecosystem scale, which was previously known at the stomatal level, with important implications for the terrestrial water cycle (Farquhar et al., 1989; Lemordant et al., 2016; Lemordant et al., 2018; Lemordant & Gentine, 2019). The estimated ecosystem conductance (G_s), that is, the inverse of r_s exhibits a VPD^{-0.5} relationship with an R^2 of 0.39 (Figure S2a), which is consistent with the Medlyn optimal stomatal model (Medlyn et al., 2011). One important point is that the r_s predictions differ across PFTs, because of the ways PFTs respond to environmental conditions, for example, SM, and different physiological characteristics, for example, vegetation height and leaf area.

One of the strengths of our approach is that we can fix environmental variables and only vary one at a time to decompose their relative contributions. We first fixed the input variables other than PFT to their mean value and evaluated the differences caused by PFT. r_s is largest for MF, followed by closed shrublands, ENF, evergreen broadleaf forests, woody savannas, deciduous broadleaf forests, GRA, savannas, and CRO, with corresponding values of 241.28, 186.51, 150.93, 140.05, 123.56, 108.91, 99.37, 99.15, and 79.57 m/s. Crops were engineered to maximize photosynthesis and therefore transpiration, explaining the low resistance of CRO.

Then we fixed the parameters in the hybrid model and assessed the sensitivity to VPD and SM, respectively, with the rest being fixed to determine which PFT has the largest VPD or SM dependence. We imposed SM to its 99th percentile value (i.e., not water stressed) for each site, WS to 1 m/s, and PAR to 1000 μmol Photon·m⁻²·s⁻¹ (i.e., saturated light conditions) and then tested which PFT had the largest VPD or SM dependence. ENF had the largest r_s dependence on VPD ($R^2 = 0.55$), while GRA had the smallest dependence on VPD ($R^2 = 0.22$) (Figure S6). Then we imposed RH to its mean value and varied SM. MF had the largest r_s dependence on SM ($R^2 = 0.45$), while CRO has the smallest r_s dependence on SM ($R^2 = 0.07$) (Figure S7).

We then test the sensitivity of the hybrid model to different environmental variables by adding a perturbation to each input variable (10–90% standard deviation increase, with 10% increment) to understand which variables are the most important regulators of r_s and LE (Figures 4a and 4b), as well as to assess their non-linearity. The most important variables (ranked by their mean R^2 with and without perturbation in Figures 4a and 4b) are h_canopy (0.80), SM (0.85), fpar (0.91), RH (0.94), Ta (0.94), Ca (0.96), WS (0.97), PAR (0.97) for LE and h_canopy (0.64), SM (0.71), fpar (0.82), Ta (0.90), RH (0.91), Ca (0.92), WS (0.94), and PAR (0.96) for r_s . Specifically, LE predictions by the hybrid model are most sensitive to h_canopy and SM. The strong dependence of ET and surface resistance on SM is well known (e.g., Akbar et al., 2019;

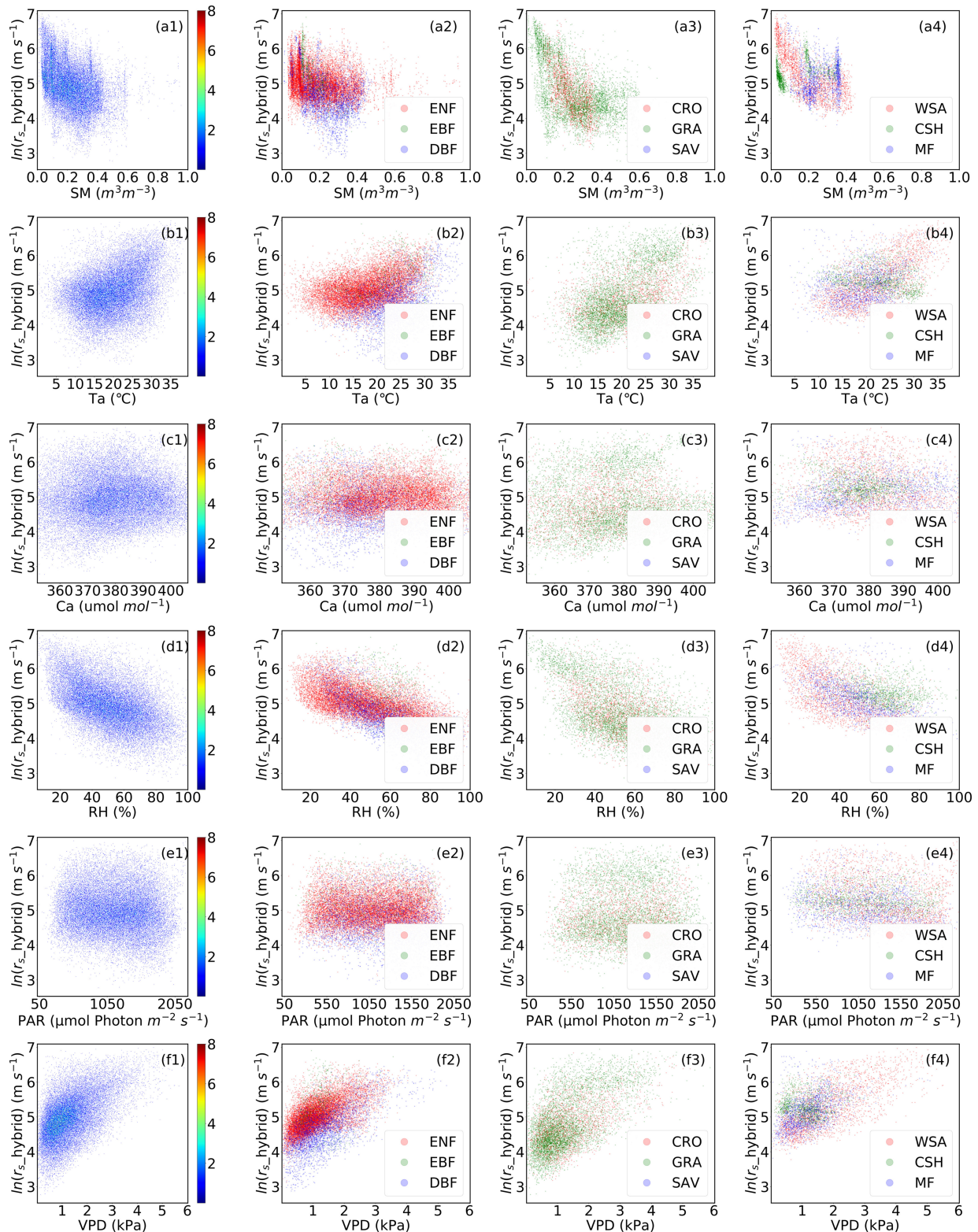


Figure 3. Density plot of the logarithmic value of predicted surface resistance (r_s) with each input variable. The temporal scale of the data is half an hour. The letters a, b, c, d, e, and f represent soil moisture (SM), air temperature (Ta), carbon dioxide concentration (Ca), relative humidity (RH), incoming photosynthetically active radiation (PAR) (incoming photosynthetic photon flux density from FLUXNET 2015 data set is used here instead), and vapor pressure deficit (VPD), respectively. The left panel, number 1, indicates that the model is used for all PFTs, and the other panels, numbers 2–4, indicate that the model is evaluated for per PFT. The density of scatter points is represented by the shading color.

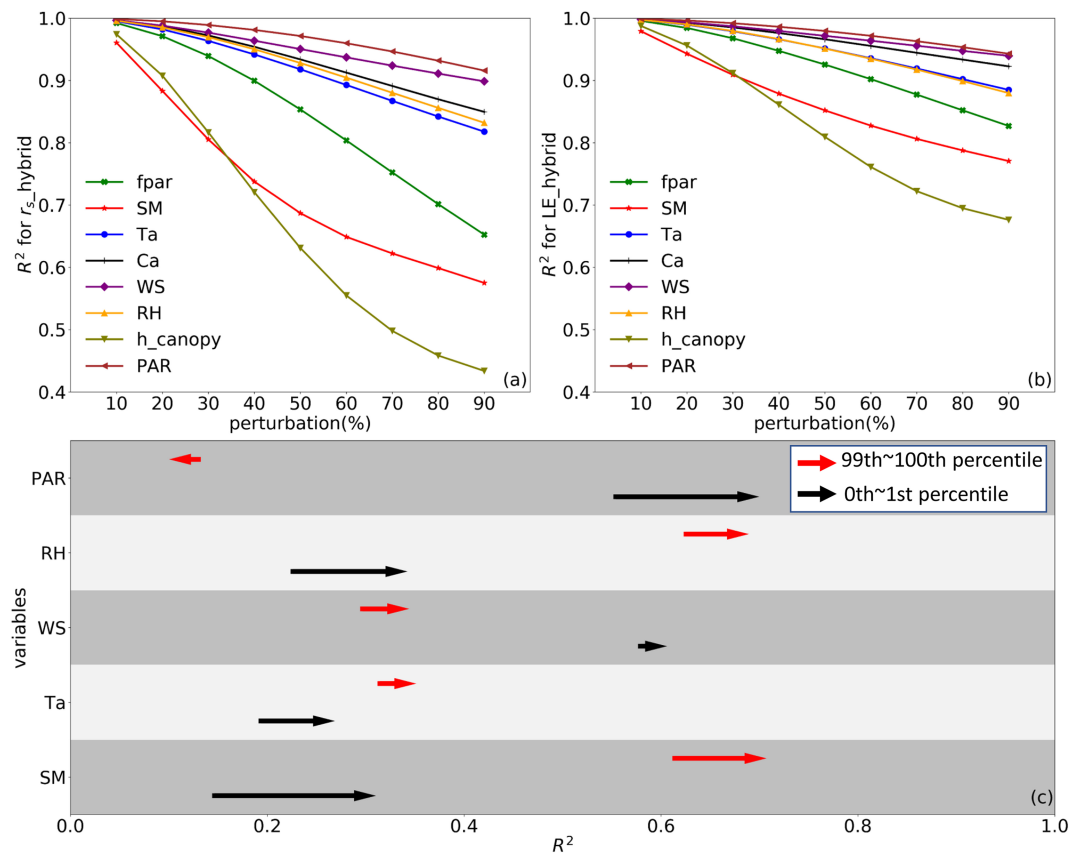


Figure 4. Interpolations and extrapolations of the hybrid and pure machine learning (ML) models. (a) Sensitivity analysis for surface resistance (r_s) predictions by hybrid model for each input variable over the test data set. 10, 20, 30, 40, 50, 60, 70, 80, and 90% standard deviation increases for each input variable. R^2 is the coefficient of determination between r_s predictions with and without perturbation. (b) Sensitivity analysis for latent heat flux (LE) predictions by hybrid model for each input variable over the test data set. (c) Performance of extrapolation for the hybrid and pure ML models over the extreme data set for all sites. R^2 is the coefficient of determination between LE predictions and observations using the extreme data set for all sites; the arrow shows the pointing R^2 change from the pure ML to the hybrid model. The red arrows indicate results using 99th~100th percentile of the data set, while black arrows are for the 0th~1st percentile extreme data set. The length of the arrow represents the R^2 difference between pure ML and hybrid model; note that for PAR the R^2 difference value is close to 0.00 for 99th~100th percentile extreme data set.

Dirmeyer, 2011; Douville et al., 2016; Entekhabi et al., 1996; Gentine et al., 2012; Koster et al., 2004; Koster et al., 2006; Seneviratne et al., 2006; Seneviratne et al., 2010; Vogel et al., 2017), but the impact of vegetation height has been only recently recognized (Groh et al., 2019; Klein et al., 2015; Ringgaard et al., 2014; Xu et al., 2018), and not thoroughly quantified. Here we find that canopy height is even more important than SM. It is not just due to the correlated effect of vegetation height with biomass, as the fpar predictive power is much lower than the vegetation canopy height. One explanation for this result is that vegetation height is strongly related to plant hydraulic traits (Giardina et al., 2018; Liu et al., 2019), which are important regulators of transpiration and thus of ET. Importantly, WS contributes very little to the r_s prediction (0.90–1.00), which indicates that for most practical applications we can eliminate WS in the prediction of r_s .

4.3. Generalizations of Hybrid and Pure ML Models

We then compare the capacity of the pure ML and hybrid models to generalize. We use the 0th~1st percentile/99th~100th percentile extremes of each data set (excluded from the training set before, Figure S3) to assess the response of each model: for instance, for SM we investigate droughts, that is, below the 1st percentile, for temperature we investigate data above the 99th percentile, that is, heat waves. A key result is that the hybrid model is systematically better than the pure ML model in predicting extreme data sets (Figure 4c). For SM and Ta in particular, that is, for droughts and heat waves, the hybrid model performs

much better than the pure ML model (with R^2 of 0.30 and 0.34, compared to 0.14 and 0.31 for pure ML model) (Figure 4c), emphasizing its capacity to better predict extreme weather event impact on ET. For the extreme cases of the 99th~100th percentile SM or 0th~1st percentile PAR and RH, the hybrid model also performs better than the pure ML model. The R^2 differences increase by 0.08 (from 0.61 to 0.7), 0.14 (from 0.55 to 0.69), and 0.11 (from 0.23 to 0.33), respectively, which indicates that the hybrid model has the potential to better predict ET on rainy days and the cloudy days as well as during the extremely dry days. This therefore means that our physics-constrained hybrid ET model performs better in extrapolation and for out-of-sample generalization than the pure ML model. This result is very encouraging as it emphasizes that combining ML with physical knowledge can lead to improved skills compared to pure ML.

5. Conclusions

In this study we developed a physics-constrained ML model for ET. The major strength of this method is that it can predict LE with similar skill as a pure ML model, yet the LE hybrid prediction can

1. conserve the surface energy budget,
2. respect the physics of evaporation (downgradient of vapor pressure), and
3. better generalize during extremes, showing the potential of such method for global monitoring during droughts and heat waves.

We further analyzed the most important variables controlling ET and found that vegetation height and SM were the most important control variables. This type of hybrid model can pave the way for new remote sensing products of ET using hybrid approaches to better detect extremes such as droughts and their impact on ecosystems.

Acknowledgments

The 2015 FLUXNET data were available online (<http://fluxnet.fluxdata.org/>). This work used eddy covariance data from the FLUXNET 2015 Tier 1 data set acquired and shared by the FLUXNET community, including these networks: AmeriFlux, AfriFlux, AsiaFlux, CarboAfrica, CarboEuropeIP, CarboItaly, CarboMont, ChinaFlux, Fluxnet-Canada, GreenGrass, ICOS, KoFlux, LBA, NECC, OzFlux-TERN, TCOS-Siberia, and USCCC. The FLUXNET eddy covariance data processing and harmonization was carried out by the European Fluxes Database Cluster, AmeriFlux Management Project, and Fluxdata project of FLUXNET, with the support of CDIAC and ICOS Ecosystem Thematic Center, and the OzFlux, ChinaFlux, and AsiaFlux offices. The fraction of photosynthetically active radiation (fpar) information was taken from simultaneous MODIS products MCD15A3H using the Global Subset Tool (<https://modis.ornl.gov/cgi-bin/MODIS/global/subset.pl>). We gratefully acknowledge the support from the Special Fund for National Key Research and Development Plan (2017FY100206-03), the Program of Science and Technology of Shenzhen (JCYJ20180504165440088), the China Scholarship Council (201806010242) for giving the opportunity to visit Columbia University. Gentine thanks funding from NASA grant 80NSSC18K0998.

References

- Akaike, H. (1974). A new look at the statistical model identification. In *Selected Papers of Hirotugu Akaike* (pp. 215–222). New York: Springer.
- Akaike, H., Parzen, E., Tanabe, K., & Kitagawa, G. (1998). *Selected papers of Hirotugu Akaike*. New York, NY: Springer Science & Business Media.
- Akbar, R., Short Gianotti, D. J., Salvucci, G. D., & Entekhabi, D. (2019). Mapped hydroclimatology of evapotranspiration and drainage runoff using SMAP brightness temperature observations and precipitation information. *Water Resources Research*, 55, 3391–3413. <https://doi.org/10.1029/2018WR024459>
- Albergel, C., Rüdiger, C., Pellarin, T., Calvet, J.-C., Fritz, N., Froissard, F., et al. (2008). From near-surface to root-zone soil moisture using an exponential filter: an assessment of the method based on in-situ observations and model simulations. *Hydrology and Earth System Sciences*, 12(6), 1323–1337. <https://doi.org/10.5194/hess-12-1323-2008>
- Alemohammad, S. H., Fang, B., Konings, A. G., Aires, F., Green, J. K., Kolassa, J., et al. (2017). Water, Energy, and Carbon with Artificial Neural Networks (WECANN): A statistically based estimate of global surface turbulent fluxes and gross primary productivity using solar-induced fluorescence. *Biogeosciences*, 14(18), 4101–4124. <https://doi.org/10.5194/bg-14-4101-2017>
- Anders, U., & Korn, O. (1999). Model selection in neural networks. *Neural Networks*, 12(2), 309–323. [https://doi.org/10.1016/S0893-6080\(98\)00117-8](https://doi.org/10.1016/S0893-6080(98)00117-8)
- Arifovic, J., & Gençay, R. (2001). Using genetic algorithms to select architecture of a feedforward artificial neural network. *Physica A: Statistical Mechanics and its Applications*, 289(3-4), 574–594. [https://doi.org/10.1016/S0378-4371\(00\)00479-9](https://doi.org/10.1016/S0378-4371(00)00479-9)
- Barr, A., Morgenstern, K., Black, T., McCaughey, J., & Nesic, Z. (2006). Surface energy balance closure by the eddy-covariance method above three boreal forest stands and implications for the measurement of the CO₂ flux. *Agricultural and Forest Meteorology*, 140(1-4), 322–337. <https://doi.org/10.1016/j.agrmet.2006.08.007>
- Bastiaanssen, W. G. M., Pelgrum, H., Wang, J., Ma, Y., Moreno, J. F., Roerink, G. J., & van der Wal, T. (1998). A remote sensing surface energy balance algorithm for land (SEBAL): Part 2: Validation. *Journal of Hydrology*, 212–213, 213–229. [https://doi.org/10.1016/S0022-1694\(98\)00254-6](https://doi.org/10.1016/S0022-1694(98)00254-6)
- Carlson, T. N., & Petropoulos, G. P. (2019). A new method for estimating of evapotranspiration and surface soil moisture from optical and thermal infrared measurements: The simplified triangle. *International Journal of Remote Sensing*, 40(20), 7716–7729. <https://doi.org/10.1080/01431161.2019.1601288>
- Chaney, N. W., Herman, J. D., Ek, M. B., & Wood, E. F. (2016). Deriving global parameter estimates for the Noah land surface model using FLUXNET and machine learning. *Journal of Geophysical Research: Atmospheres*, 121, 13,218–213,235. <https://doi.org/10.1002/2016JD024821>
- Cleugh, H. A., Leuning, R., Mu, Q., & Running, S. W. (2007). Regional evaporation estimates from flux tower and MODIS satellite data. *Remote Sensing of Environment*, 106(3), 285–304. <https://doi.org/10.1016/j.rse.2006.07.007>
- Dirmeyer, P. A. (2011). The terrestrial segment of soil moisture–climate coupling. *Geophysical Research Letters*, 38, L16702. <https://doi.org/10.1029/2011GL048268>
- Douville, H., Colin, J., Krug, E., Cattiaux, J., & Thao, S. (2016). Midlatitude daily summer temperatures reshaped by soil moisture under climate change. *Geophysical Research Letters*, 43, 812–818. <https://doi.org/10.1002/2015GL066222>
- Entekhabi, D., Rodriguez-Iturbe, I., & Castelli, F. (1996). Mutual interaction of soil moisture state and atmospheric processes. *Journal of Hydrology*, 184(1-2), 3–17. [https://doi.org/10.1016/0022-1694\(95\)02965-6](https://doi.org/10.1016/0022-1694(95)02965-6)
- Farquhar, G. D., Ehleringer, J. R., & Hubick, K. T. (1989). Carbon isotope discrimination and photosynthesis. *Annual Review of Plant Biology*, 40(1), 503–537. <https://doi.org/10.1146/annurev.pp.40.060189.002443>

- Feng, Y., Peng, Y., Cui, N., Gong, D., & Zhang, K. (2017). Modeling reference evapotranspiration using extreme learning machine and generalized regression neural network only with temperature data. *Computers and Electronics in Agriculture*, 136, 71–78. <https://doi.org/10.1016/j.compag.2017.01.027>
- Ford, T., Harris, E., & Quiring, S. (2014). Estimating root zone soil moisture using near-surface observations from SMOS. *Hydrology and Earth System Sciences*, 18(1), 139–154. <https://doi.org/10.5194/hess-18-139-2014>
- Gao, W. (1988). Applications of solutions to non-linear energy budget equations. *Agricultural and Forest Meteorology*, 43(2), 121–145. [https://doi.org/10.1016/0168-1923\(88\)90087-1](https://doi.org/10.1016/0168-1923(88)90087-1)
- Gentine, P., D'Odorico, P., Lintner, B. R., Sivandran, G., & Salvucci, G. (2012). Interdependence of climate, soil, and vegetation as constrained by the Budkyo curve. *Geophysical Research Letters*, 39, L19404. <https://doi.org/10.1029/2012GL053492>
- Giardina, F., Konings, A. G., Kennedy, D., Aleomohammad, S. H., Oliveira, R. S., Uriarte, M., & Gentine, P. (2018). Tall Amazonian forests are less sensitive to precipitation variability. *Nature Geoscience*, 11(6), 405–409. <https://doi.org/10.1038/s41561-018-0133-5>
- Gocic, M., Petković, D., Shamshirband, S., & Kamsin, A. (2016). Comparative analysis of reference evapotranspiration equations modelling by extreme learning machine. *Computers and Electronics in Agriculture*, 127, 56–63. <https://doi.org/10.1016/j.compag.2016.05.017>
- Granata, F. (2019). Evapotranspiration evaluation models based on machine learning algorithms—A comparative study. *Agricultural Water Management*, 217, 303–315. <https://doi.org/10.1016/j.agwat.2019.03.015>
- Groh, J., Pütz, T., Gerke, H., Vanderborght, J., & Vereecken, H. (2019). Quantification and prediction of nighttime evapotranspiration for two distinct grassland ecosystems. *Water Resources Research*, 55(4), 2961–2975. <https://doi.org/10.1029/2018WR024072>
- Jarvis, P. (1976). The interpretation of the variations in leaf water potential and stomatal conductance found in canopies in the field. *Philosophical Transactions of the Royal Society of London. B, Biological Sciences*, 273(927), 593–610. <https://doi.org/10.1098/rstb.1976.0035>
- Jiang, L., & Islam, S. (1999). A methodology for estimation of surface evapotranspiration over large areas using remote sensing observations. *Geophysical Research Letters*, 26(17), 2773–2776. <https://doi.org/10.1029/1999GL006049>
- Jung, M., Reichstein, M., & Bondeau, A. (2009). Towards global empirical upscaling of FLUXNET eddy covariance observations: Validation of a model tree ensemble approach using a biosphere model. *Biogeosciences*, 6(10), 2001–2013. <https://doi.org/10.5194/bg-6-2001-2009>
- Jung, M., Reichstein, M., Ciais, P., Seneviratne, S. I., Sheffield, J., Goulden, M. L., et al. (2010). Recent decline in the global land evapotranspiration trend due to limited moisture supply. *Nature*, 467(7318), 951–954. <https://doi.org/10.1038/nature09396>
- Katul, G. G., Oren, R., Manzoni, S., Higgins, C., & Parlange, M. B. (2012). Evapotranspiration: a process driving mass transport and energy exchange in the soil-plant-atmosphere-climate system. *Reviews of Geophysics*, 50, RG3002. <https://doi.org/10.1029/2011RG000366>
- Ke, Y., Im, J., Park, S., & Gong, H. (2016). Downscaling of MODIS One kilometer evapotranspiration using Landsat-8 data and machine learning approaches. *Remote Sensing*, 8(3), 215. <https://doi.org/10.3390/rs8030215>
- Klein, T., Randin, C., & Körner, C. (2015). Water availability predicts forest canopy height at the global scale. *Ecology Letters*, 18(12), 1311–1320. <https://doi.org/10.1111/ele.12525>
- Koster, R. D., Dirmeyer, P. A., Guo, Z., Bonan, G., Chan, E., Cox, P., et al. (2004). Regions of strong coupling between soil moisture and precipitation. *Science*, 305(5687), 1138–1140. <https://doi.org/10.1126/science.1100217>
- Koster, R. D., Sud, Y., Guo, Z., Dirmeyer, P. A., Bonan, G., Oleson, K. W., et al. (2006). GLACE: The global land–atmosphere coupling experiment. Part I: overview. *Journal of Hydrometeorology*, 7(4), 590–610. <https://doi.org/10.1175/JHM510.1>
- Lemordant, L., & Gentine, P. (2019). Vegetation response to rising CO₂ impacts extreme temperatures. *Geophysical Research Letters*, 46, 1383–1392. <https://doi.org/10.1029/2018GL080238>
- Lemordant, L., Gentine, P., Stéfanon, M., Drobinski, P., & Faticchi, S. (2016). Modification of land-atmosphere interactions by CO₂ effects: Implications for summer dryness and heat wave amplitude. *Geophysical Research Letters*, 43, 10,240–10,248. <https://doi.org/10.1002/2016GL069896>
- Lemordant, L., Gentine, P., Swann, A. S., Cook, B. I., & Scheff, J. (2018). Critical impact of vegetation physiology on the continental hydrologic cycle in response to increasing CO₂. *Proceedings of the National Academy of Sciences*, 115(16), 4093–4098. <https://doi.org/10.1073/pnas.1720712115>
- Leuning, R., Zhang, Y. Q., Rajaud, A., Cleugh, H., & Tu, K. (2008). A simple surface conductance model to estimate regional evaporation using MODIS leaf area index and the Penman-Monteith equation. *Water Resources Research*, 44, W10419. <https://doi.org/10.1029/2007WR006562>
- Li, X., Gentine, P., Lin, C., Zhou, S., Sun, Z., Zheng, Y., et al. (2019). A simple and objective method to partition evapotranspiration into transpiration and evaporation at eddy-covariance sites. *Agricultural and Forest Meteorology*, 265, 171–182. <https://doi.org/10.1016/j.agrformet.2018.11.017>
- Li, Y., Kustas, W. P., Huang, C., Nieto, H., Haghghi, E., Anderson, M. C., et al. (2019). Evaluating soil resistance formulations in thermal-based Two-Source Energy Balance (TSEB) model: Implications for heterogeneous semiarid and arid regions. *Water Resources Research*, 55, 1059–1078. <https://doi.org/10.1029/2018WR022981>
- Lin, C., Gentine, P., Huang, Y., Guan, K., Kimm, H., & Zhou, S. (2018). Diel ecosystem conductance response to vapor pressure deficit is suboptimal and independent of soil moisture. *Agricultural and Forest Meteorology*, 250–251, 24–34. <https://doi.org/10.1016/j.agrformet.2017.12.078>
- Liu, H., Gleason, S. M., Hao, G., Hua, L., He, P., Goldstein, G., & Ye, Q. (2019). Hydraulic traits are coordinated with maximum plant height at the global scale. *Science Advances*, 5, eaav1332. <https://doi.org/10.1126/sciadv.aav1332>
- Liu, S. M., Xu, Z. W., Wang, W. Z., Jia, Z. Z., Zhu, M. J., Bai, J., & Wang, J. M. (2011). A comparison of eddy-covariance and large aperture scintillometer measurements with respect to the energy balance closure problem. *Hydrology and Earth System Sciences*, 15(4), 1291–1306. <https://doi.org/10.5194/hess-15-1291-2011>
- Long, D., & Singh, V. P. (2012). A Two-source Trapezoid Model for Evapotranspiration (TTME) from satellite imagery. *Remote Sensing of Environment*, 121, 370–388. <https://doi.org/10.1016/j.rse.2012.02.015>
- Loveland, T. R., Zhu, Z., Ohlen, D. O., Brown, J. F., Reed, B. C., & Yang, L. (1999). An analysis of the IGBP global land-cover characterization process. *Photogrammetric engineering and remote sensing*, 65, 1021–1032.
- McCabe, M. F., & Wood, E. F. (2006). Scale influences on the remote estimation of evapotranspiration using multiple satellite sensors. *Remote Sensing of Environment*, 105(4), 271–285. <https://doi.org/10.1016/j.rse.2006.07.006>
- Medlyn, B. E., Duursma, R. A., Eamus, D., Ellsworth, D. S., Prentice, I. C., Barton, C. V., et al. (2011). Reconciling the optimal and empirical approaches to modelling stomatal conductance. *Global Change Biology*, 17(6), 2134–2144. <https://doi.org/10.1111/j.1365-2486.2010.02375.x>
- Monteith, J. L. (1965). *Evaporation and environment*, paper presented at Symposia of the society for experimental biology. Cambridge: Cambridge University Press (CUP).

- Morillas, L., Leuning, R., Villagarcía, L., García, M., Serrano-Ortíz, P., & Domingo, F. (2013). Improving evapotranspiration estimates in Mediterranean drylands: The role of soil evaporation. *Water Resources Research*, 49, 6572–6586. <https://doi.org/10.1002/wrcr.20468>
- Mu, Q., Heinsch, F. A., Zhao, M., & Running, S. W. (2007). Development of a global evapotranspiration algorithm based on MODIS and global meteorology data. *Remote sensing of Environment*, 111(4), 519–536. <https://doi.org/10.1016/j.rse.2007.04.015>
- Mu, Q., Zhao, M., & Running, S. W. (2011). Improvements to a MODIS global terrestrial evapotranspiration algorithm. *Remote Sensing of Environment*, 115(8), 1781–1800. <https://doi.org/10.1016/j.rse.2011.02.019>
- Norman, J. M., Kustas, W. P., & Humes, K. S. (1995). Source approach for estimating soil and vegetation energy fluxes in observations of directional radiometric surface temperature. *Agricultural and Forest Meteorology*, 77(3-4), 263–293. [https://doi.org/10.1016/0168-1923\(95\)02265-Y](https://doi.org/10.1016/0168-1923(95)02265-Y)
- Peng, L., Zeng, Z., Wei, Z., Chen, A., Wood, E. F., & Sheffield, J. (2019). Determinants of the ratio of actual to potential evapotranspiration. *Global change biology*, 25(4), 1326–1343. <https://doi.org/10.1111/gcb.14577>
- Penman, H. L. (1948). Natural evaporation from open water, bare soil and grass. *Proceedings of the Royal Society of London. Series A. Mathematical and Physical Sciences*, 193(1032), 120–145. <https://doi.org/10.1098/rspa.1948.0037>
- Pennypacker, S., & Baldocchi, D. (2016). Seeing the fields and forests: Application of surface-layer theory and flux-tower data to calculating vegetation canopy height. *Boundary-layer meteorology*, 158(2), 165–182. <https://doi.org/10.1007/s10546-015-0090-0>
- Qiu, G. Y. (1996). Estimation of plant transpiration by imitation leaf temperature II. application of imitation leaf temperature for detection of crop water stress. *Transactions of the Japanese society of irrigation, drainage and reclamation engineering*, 64(5), 767–773.
- Qiu, G. Y., Momii, K., & Yano, T. (1996). Estimation of plant transpiration by imitation leaf temperature. *Transactions of the Japanese society of irrigation, Drainage and Reclamation Engineering*, 1996(183), 401–410, a401. <https://doi.org/10.11408/jsidre1965.1996.401>
- Qiu, J., Crow, W. T., Nearing, G. S., Mo, X., & Liu, S. (2014). The impact of vertical measurement depth on the information content of soil moisture times series data. *Geophysical Research Letters*, 41, 4997–5004. <https://doi.org/10.1002/2014GL060017>
- Reichstein, M., Bahn, M., Mahecha, M. D., Kattge, J., & Baldocchi, D. D. (2014). Linking plants and ecosystem functional biogeography. *Proceedings of the National Academy of Sciences*, 111(38), 13,697–13,702. <https://doi.org/10.1073/pnas.1216065111>
- Reichstein, M., Camps-Valls, G., Stevens, B., Jung, M., Denzler, J., & Carvalhais, N. (2019). Deep learning and process understanding for data-driven Earth system science. *Nature*, 566(7743), 195–204. <https://doi.org/10.1038/s41586-019-0912-1>
- Reichstein, M., Falge, E., Baldocchi, D., Papale, D., Aubinet, M., Berbigier, P., et al. (2005). On the separation of net ecosystem exchange into assimilation and ecosystem respiration: review and improved algorithm. *Global Change Biology*, 11(9), 1424–1439. <https://doi.org/10.1111/j.1365-2486.2005.001002.x>
- Ringgaard, R., Herbst, M., & Friberg, T. (2014). Partitioning forest evapotranspiration: Interception evaporation and the impact of canopy structure, local and regional advection. *Journal of Hydrology*, 517, 677–690. <https://doi.org/10.1016/j.jhydrol.2014.06.007>
- Seneviratne, S. I., Corti, T., Davin, E. L., Hirschi, M., Jaeger, E. B., Lehner, I., et al. (2010). Investigating soil moisture–climate interactions in a changing climate: A review. *Earth-Science Reviews*, 99(3-4), 125–161. <https://doi.org/10.1016/j.earscirev.2010.02.004>
- Seneviratne, S. I., Lüthi, D., Litschi, M., & Schär, C. (2006). Land–atmosphere coupling and climate change in Europe. *Nature*, 443(7108), 205–209. <https://doi.org/10.1038/nature05095>
- Tang, D., Feng, Y., Gong, D., Hao, W., & Cui, N. (2018). Evaluation of artificial intelligence models for actual crop evapotranspiration modeling in mulched and non-mulched maize croplands. *Computers and electronics in agriculture*, 152, 375–384. <https://doi.org/10.1016/j.compag.2018.07.029>
- Torres, A. F., Walker, W. R., & McKee, M. (2011). Forecasting daily potential evapotranspiration using machine learning and limited climatic data. *Agricultural Water Management*, 98(4), 553–562. <https://doi.org/10.1016/j.agwat.2010.10.012>
- Tramontana, G., Jung, M., Camps-Valls, G., Ichii, K., Ráduly, B., Reichstein, M., et al. (2016). Predicting carbon dioxide and energy fluxes across global FLUXNET sites with regression algorithms. *Biogeosciences Discussions*, 13(14), 4291–4313. <https://doi.org/10.5194/bg-13-4291-2016>
- Twine, T. E., Kustas, W., Norman, J., Cook, D., Houser, P., Meyers, T., et al. (2000). Correcting eddy-covariance flux underestimates over a grassland. *Agricultural and Forest Meteorology*, 103(3), 279–300. [https://doi.org/10.1016/S0168-1923\(00\)00123-4](https://doi.org/10.1016/S0168-1923(00)00123-4)
- Vogel, M. M., Orth, R., Cheruy, F., Hagemann, S., Lorenz, R., van den Hurk, B. J., & Seneviratne, S. I. (2017). Regional amplification of projected changes in extreme temperatures strongly controlled by soil moisture–temperature feedbacks. *Geophysical Research Letters*, 44, 1511–1519. <https://doi.org/10.1002/2016GL071235>
- Wang, K., & Dickinson, R. E. (2012). A review of global terrestrial evapotranspiration: Observation, modeling, climatology, and climatic variability. *Reviews of Geophysics*, 50, RG2005. <https://doi.org/10.1029/2011RG000373>
- Wang, K., Wang, P., Li, Z., Cribb, M., & Sparrow, M. (2007). A simple method to estimate actual evapotranspiration from a combination of net radiation, vegetation index, and temperature. *Journal of Geophysical Research*, 112, D15107. <https://doi.org/10.1029/2006JD008351>
- Wang, Y. Q., Xiong, Y. J., Qiu, G. Y., & Zhang, Q. T. (2016). Is scale really a challenge in evapotranspiration estimation? A multi-scale study in the Heihe oasis using thermal remote sensing and the three-temperature model. *Agricultural and Forest Meteorology*, 230–231, 128–141. <https://doi.org/10.1016/j.agrformet.2016.03.012>
- Xu, D., Agee, E., Wang, J., & Ivanov, V. Y. (2019). Estimation of evapotranspiration of Amazon rainforest using the maximum entropy production method. *Geophysical Research Letters*, 46, 1402–1412. <https://doi.org/10.1029/2018GL080907>
- Xu, P., Zhou, T., Yi, C., Fang, W., Hendrey, G., & Zhao, X. (2018). Forest drought resistance distinguished by canopy height. *Environmental Research Letters*, 13, 075003. <https://doi.org/10.1088/1748-9326/aacd>
- Xu, Z., Liu, S., Li, X., Shi, S., Wang, J., Zhu, Z., et al. (2013). Intercomparison of surface energy flux measurement systems used during the HiWATER-MUSOEXE. *Journal of Geophysical Research: Atmospheres*, 118, 13,140–13,157. <https://doi.org/10.1002/2013JD020260>
- Yang, F., White, M. A., Michaelis, A. R., Ichii, K., Hashimoto, H., Votava, P., et al. (2006). Prediction of continental-scale evapotranspiration by combining MODIS and AmeriFlux data through support vector machine. *IEEE Transactions on Geoscience and Remote Sensing*, 44(11), 3452–3461. <https://doi.org/10.1109/TGRS.2006.876297>
- Yang, Y., & Shang, S. (2013). A hybrid dual-source scheme and trapezoid framework-based evapotranspiration model (HTEM) using satellite images: Algorithm and model test. *Journal of Geophysical Research: Atmospheres*, 118, 2284–2300. <https://doi.org/10.1002/jgrd.50259>
- Yao, Y., Liang, S., Li, X., Chen, J., Wang, K., Jia, K., et al. (2015). A satellite-based hybrid algorithm to determine the Priestley–Taylor parameter for global terrestrial latent heat flux estimation across multiple biomes. *Remote Sensing of Environment*, 165, 216–233. <https://doi.org/10.1016/j.rse.2015.05.013>
- Zhang, K., Kimball, J. S., Nemani, R. R., & Running, S. W. (2010). A continuous satellite-derived global record of land surface evapotranspiration from 1983 to 2006. *Water Resources Research*, 46, W09522. <https://doi.org/10.1029/2009WR008800>

- Zhang, K., Kimball, J. S., & Running, S. W. (2016). A review of remote sensing based actual evapotranspiration estimation. *Wiley Interdisciplinary Reviews: Water*, 3(6), 834–853. <https://doi.org/10.1002/wat2.1168>
- Zhang, K., Zhu, G., Ma, J., Yang, Y., Shang, S., & Gu, C. (2019). Parameter analysis and estimates for the MODIS evapotranspiration algorithm and multiscale verification. *Water Resources Research*, 55, 2211–2231. <https://doi.org/10.1029/2018WR023485>
- Zhou, S., Yu, B., Huang, Y., & Wang, G. (2015). Daily underlying water use efficiency for AmeriFlux sites. *Journal of Geophysical Research: Biogeosciences*, 120, 887–902. <https://doi.org/10.1002/2015JG002947>
- Zhou, S., Yu, B., Zhang, Y., Huang, Y., & Wang, G. (2016). Partitioning evapotranspiration based on the concept of underlying water use efficiency. *Water Resources Research*, 52, 1160–1175. <https://doi.org/10.1002/2015WR017766>
- Zhu, W., Lv, A., Jia, S., & Yan, J. (2017). A new contextual parameterization of evaporative fraction to reduce the reliance of the Ts – VI triangle method on the dry edge. *Remote Sensing*, 9(1), 26. <https://doi.org/10.3390/rs9010026>
- Zou, Z., Yang, Y., & Qiu, G. Y. (2019). Quantifying the evapotranspiration rate and its cooling effects of urban hedges based on three-temperature model and infrared remote sensing. *Remote Sensing*, 11(2), 202. <https://doi.org/10.3390/rs11020202>